Attosecond Photoscopy of Plasmonic Excitations

Mattia Lupetti,[1,*] Julia Hengster,[2] Thorsten Uphues,[2] and Armin Scrinzi[1,†]
[1]*Physics Department, Ludwig Maximilians Universität, D-80333 Munich, Germany*
[2]*Center for Free-Electron Laser Science, Universität Hamburg, D-22761 Hamburg, Germany*
(Received 20 January 2014; published 12 September 2014)

We propose an experimental arrangement to image, with attosecond resolution, transient surface plasmonic excitations. The required modifications to state-of-the-art setups used for attosecond streaking experiments from solid surfaces only involve available technology. Buildup and lifetimes of surface plasmon polaritons can be extracted and local modulations of the exciting optical pulse can be diagnosed *in situ*.

DOI: 10.1103/PhysRevLett.113.113903 PACS numbers: 42.65.Ky, 32.80.Rm, 42.65.Re

Surface plasmons are collective excitations of electrons that propagate along a metal-dielectric interface. Recently, plasmonics has gathered interest for the development of ultrafast all-optical circuitry [1], since it can combine the high operational speed of photonics (PHz scale) with the miniaturization provided by electronics (nm scale). For this purpose, it is important to understand the buildup dynamics and lifetime of the collective electronic excitation. Although the plasmon lifetime can be inferred from the plasmonic resonance width (of the transmission spectrum, see, for instance, [2]), plasmon buildup is a process that cannot be addressed in terms of frequency analysis.

In the present Letter, we propose an experimental setup to image the transient dynamics of a plasmonic mode, which can be realized as a modification of the so-called "attosecond streak camera" [3], which has already been successfully applied to solid surfaces. The attosecond streak camera is a two-color pump-probe scheme, where a weak extreme ultraviolet (XUV) attosecond pulse ionizes electrons from the solid, and a collinear, few-cycle (∼5 fs FWHM) near-infrared (NIR) pulse serves as the probe, which accelerates the XUV photoelectrons after their escape from the solid. With this technique it was possible to resolve solid-state physics phenomena with resolution of a few attoseconds (1 as $= 10^{-18}$ s) [4].

We benchmark our setup concept against the buildup of surface plasmon polaritons (SPPs) excited by a NIR pulse on a grating surface. A time-delayed XUV pulse probes the SPPs during their evolution by detecting the effect of their field on XUV photoemission. In principle, pump and probe beams can be spatially separated, allowing us to probe different surface regions. Thus, differently from atomic and surface streaking employed so far, the setup provides spatiotemporal information. To distinguish it from standard attosecond streaking experiments, we name our setup "attosecond photoscopy."

A well established method for producing isolated attosecond pulses is the generation of high harmonic radiation in noble gases [4–7]. An intense few cycle NIR laser pulse is focused into a noble gas target and generates high harmonics of the fundamental radiation. The XUV radiation copropagates with the driving laser pulse. Both pulses are focused onto a sample with a delayable two part mirror composed of an XUV multilayer mirror in the inner part and a broadband NIR mirror in the outer part. The multilayer mirror is designed as a band pass filter for the harmonics, which results in an isolated attosecond pulse. The pulse can be timed relative to the NIR with a precision of $\lesssim$10 as.

Figure 1 illustrates the setup discussed here. The NIR and XUV beams propagate in the y direction, at normal incidence onto the plane of the grating. Polarizations are in the x direction, perpendicular to the grooves. Using this arrangement, two counterpropagating plasmons are excited in the focus of the NIR pulse on the grating structure. A band gap at the zero crossing separates two plasmon branches [8]. An optical pulse at normal incidence usually couples to only one of the branches, called the bright mode, but, at tight focussing with about 5° angular dispersion, the second, "dark" mode is also excited.

XUV photoelectrons are measured at a direction perpendicular to the surface. As in [4], the final electron

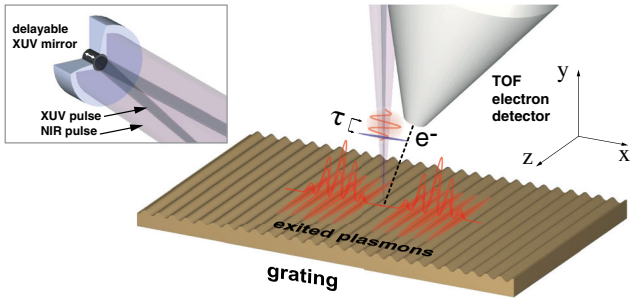

FIG. 1 (color online). Experimental setup of an attosecond photoscopy experiment. The XUV attosecond pulse liberates electrons in the presence of the plasmonic field, which is excited by a short NIR pulse. Control of NIR-XUV time delay τ allows observation of the plasmon transient dynamics.

momenta are recorded as a function of the delay between the NIR and XUV beams. The electron spectrogram retrieved is a convolution of photoemission with acceleration in the plasmonic field at the location and time of the initial electron release.

Depending on the time delay between the NIR pulse and the probing attosecond pulse, the XUV generated photoelectrons experience a different plasmonic field amplitude and phase, leading to a modulation of the kinetic energy distribution by the emerging plasmonic field.

The energy gap between dark and bright modes manifests itself in the spectrogram as a "transition" from the bright ω_b to the dark ω_d mode frequencies, which is measurable in our setup because of the attosecond resolution.

Below, we analyze the photoscopic spectrogram using a basic analytical model as well as numerical solutions of the SPP propagation together with a Monte Carlo simulation of the electron streaking process. We will demonstrate that one can recover the plasmonic field at the surface from the spectrograms. The detailed analysis and interpretation will be discussed in the following.

Standard streaking experiments are based on electron sources that can be considered pointlike with respect to the laser wavelength, such as atoms or molecules. For this reason, the dipole approximation can be used: $\mathbf{A}(\mathbf{r},t) \simeq \mathbf{A}(t)$. After emission, the electron canonical momentum is conserved: $\mathbf{P}(t) = \mathbf{P}_i$, which translates into $\mathbf{p}(t) + (e/c)\mathbf{A}(t) = \mathbf{p}_i + (e/c)\mathbf{A}(t_i)$, where e denotes the electron charge and $|\mathbf{p}_i| = \sqrt{2m(E_{\mathrm{XUV}} - W_f)}$ is the initial momentum of the electron released at time t_i from a material with work function W_f. Assuming that $A(t \to \infty) = 0$, the final momentum recorded by the spectrometer is

$$\mathbf{p}_f = \mathbf{p}_i + \mathbf{a}(t_i), \tag{1}$$

where we defined $\mathbf{a} := (e/c)\mathbf{A}$.

The spectral width of the XUV attosecond pulse is reflected in a momentum broadening of the initial electron distribution $n_e = n_e(\mathbf{p}_i, t_i)$. For simplicity, we assume Gaussian distributions centered around momentum $\mathbf{p}_0$ and time t_0, respectively, where t_0 denotes the time of peak XUV intensity on target. With Eq. (1) for the initial electron momentum, the time-integrated final momentum is

$$\sigma(\mathbf{p}_f) = \int_{-\infty}^{\infty} dt_i n_e[\mathbf{p}_f - \mathbf{a}(t_i), t_i]. \tag{2}$$

The spectrogram for a series of delays τ becomes

$$\sigma(\mathbf{p}_f, \tau) = \int_{-\infty}^{\infty} dt_i n_e[\mathbf{p}_f - \mathbf{a}(t_i), t_i - \tau]. \tag{3}$$

From this, the NIR pulse can be reconstructed by analyzing the average momentum of the streaking spectrogram.

When applying the method to plasmonic excitations, we have to consider that the SPP, acting as the streaking field, is spatially inhomogeneous and propagates on a surface. Previous work on streaking on nanoparticles [9] clearly shows that spatial inhomogeneity of the streaking field leads to a smearing of the streaking trace obtained in a traditional setup. Thus, we need to include the position dependence into our initial electron distribution: $n_e(\mathbf{p}_i, t_i) \to n_e(\mathbf{r}_i, \mathbf{p}_i, t_i)$. The final momentum of the electrons accelerated in the plasmon field is then

$$\mathbf{p}_f = \mathbf{p}_i - e \int_{-\infty}^{\infty} \mathbf{E}(\mathbf{r}(t'), t') dt'. \tag{4}$$

For a typical XUV photon energy of 80 eV, the average initial speed of a photoelectron is $v_i = 5$ nm/fs. If the NIR pulse is 4 fs short, it will give rise to a plasmonic field of a duration of a few tens of femtoseconds. During this time, the electrons move by $\lesssim$100 nm. The additional drift imparted by the plasmonic field is small compared to the initial velocity. As the plasmon evanescent field extends to about NIR wavelength (800 nm) beyond the surface, we can write $\mathbf{r}(t') \simeq \mathbf{r}_i$ in Eq. (4). With this approximation, one obtains a position corrected analog of Eq. (1)

$$\mathbf{p}_f = \mathbf{p}_i - \mathbf{a}(\mathbf{r}_i, t_i). \tag{5}$$

Since the photoelectron detector does not resolve the emission positions $\mathbf{r}_i$, the photoscopic spectrogram is the integral over time and the area covered by the XUV pulse

$$\sigma(\mathbf{p}_f, \tau) = \int_{\mathbb{R}^3} d^3 r_i \int_{-\infty}^{\infty} dt_i n_e[\mathbf{r}_i, \mathbf{p}_f - \mathbf{a}(\mathbf{r}_i, t_i), t_i - \tau]. \tag{6}$$

The space-averaged momentum is independent of the time delay, as the integral of a propagating pulse is negligible (exactly zero in free space). Thus, for extracting time information from the photoscopic spectrogram, we use the delay-dependent momentum variance

$$S(\tau) = \frac{\int d\mathbf{p}_f |\mathbf{p}_f|^2 \sigma(\mathbf{p}_f, \tau)}{\int d\mathbf{p}_f \sigma(\mathbf{p}_f, \tau)} - |\langle \mathbf{p}_f \rangle|^2. \tag{7}$$

As the XUV pulse duration is short compared to the NIR period, we treat photoemission as instantaneous. The distribution of the photoelectron yield along the surface is proportional to the XUV intensity profile. Furthermore, we neglect any transport effect in the solid and consider only the photoelectrons coming from the first few layers of material, as reported in [10]. With these conditions, one finds

$$n_e(\mathbf{r}_i, \mathbf{p}_i, t_i - \tau) \simeq g_{\mathrm{x}}(x_i) n_e(\mathbf{p}_i) \delta(y_i - y_s) \delta(t_i - \tau - t_0),$$

where y_s is the grating vertical position (we neglect any groove depth effect) and g_{x} is a Gaussian function of width w_{x}, i.e., the XUV attosecond pulse focal spot.

As for the angular dependence of the photoemission, we first restrict our discussion to the two extreme cases of (1) unidirectional emission with all initial momenta orthogonal to the grating plane, and (2) isotropic emission. For either distribution, the reconstructed times closely reproduce the actual dynamics. In reality, the XUV photoelectron distribution will be between these extreme cases and should be determined in a measurement without a NIR field.

Unidirectional initial distributions can be written as $n_e(\mathbf{p}_i) = n_e(p_i\hat{\mathbf{n}}_s)$, where $p_i = |\mathbf{p}_i|$ and $\hat{\mathbf{n}}_s$ is the direction orthogonal to the grating plane. Equation (6) now becomes

$$\sigma(p_f,\tau) = \int_{-\infty}^{\infty} dx_i g_x(x_i) n_e[p_f - \hat{\mathbf{n}}_s \cdot \mathbf{a}(x_i, t_0 - \tau)],$$

where $\hat{\mathbf{n}}_s$ denotes the surface normal. Near the surface, in the region that is probed by the electrons, the plasmonic field is predominantly perpendicular to the surface. Therefore, we can approximate $\hat{\mathbf{n}}_s \cdot \mathbf{a} = \mathsf{a}_y \simeq \mathsf{a}_{\mathrm{SPP}}$. Computing the variance Eq. (7) for a Gaussian distribution of the initial electron momenta, we obtain

$$S(\tau) = \Delta p^2 + \int_{-\infty}^{\infty} dx_i g_x(x_i) \mathsf{a}^2_{\mathrm{SPP}}(x_i, t_0 - \tau). \quad (8)$$

For isotropic XUV photoelectron emission, the initial distribution can be written as $n_e(\mathbf{p}_i) = (1/\pi) n_e(p_i) = (1/\pi) n_e(|\mathbf{p}_f - \mathbf{a}|)$, where we employed $p_i = |\mathbf{p}_i|$. We use $|\mathbf{a}| \ll |\mathbf{p}_f|$ to approximate $|\mathbf{p}_f - \mathbf{a}| \simeq p_f - \mathbf{a}\cdot\hat{\theta}$, where θ is the angle between the final momentum and the surface normal. The spectrogram then reads

$$\sigma(p_f,\tau) = \frac{1}{\pi}\int_{-\infty}^{\infty} dx_i g_x(x_i) n_e(p_f - \mathbf{a}\cdot\hat{\theta}). \quad (9)$$

A straightforward calculation for the angular integrations leads to the expression of the variance

$$S(\tau) = \Delta p^2 + \frac{1}{\pi}\int_{-\infty}^{\infty} dx_i g_x(x_i) |\mathbf{a}(x_i,\tau)|^2. \quad (10)$$

In either case, by Eqs. (8) and (10), measuring the variance of the photoemission spectrogram provides direct access to the space-averaged vector potential $\mathbf{a}^2$ at the surface in the direction of photodetection. The surface vector potential $|\mathbf{a}|^2 = \mathsf{a}_x^2 + \mathsf{a}^2_{\mathrm{SPP}}$ also includes a_x, the NIR field at the grating surface. Modifications of the surface field compared to the incident beam can be measured *in situ* (see below).

Simulations of the plasmonic field were performed with the finite-difference time-domain (FDTD) method [11], using a freely available software package [12]. Material properties were included through the appropriate model of gold dielectric function [13]. We assume a Gaussian 4 fs FWHM pulse at a central wavelength of 800 nm. The grating parameters are optimized for maximal absorption from the NIR pulse, assuming a gold surface. Beam waists of NIR and XUV were 5 and 10 μm, respectively.

The XUV photoemission process is approximated as a sudden ejection of electrons from the surface boundary, with the appropriate unidirectional and isotropic initial momentum distribution. The electron trajectories and final momenta are computed by solving the Lorentz equation for each photoelectron in the previously simulated electromagnetic field.

The spectrogram variance obtained by Monte Carlo simulation is compared in Fig. 2 with the space integral of the squared vector potential along y from the FDTD simulation. We assume isotropic initial momentum distribution and a TOF detector of 5° acceptance centered around the perpendicular direction.

Note that the variance directly images the integral of the surface plasmonic field squared without further assumptions or input from theory. The agreement is robust with respect to the angular distribution of photoelectron momenta: one obtains analogous results for unidirectional emission.

The detailed image of the fields provides for an *in situ* diagnosis of both, plasmon field and exciting NIR source, including possible distortions due to the NIR reflection on the grating. In Figure 3, spectrograms observed in the perpendicular and grazing direction are shown, which reflect the two contributions.

From the plasmonic (perpendicular) component, we extract buildup and lifetimes, as well as contributions of the bright and dark modes to the spectrograms. We parametrize the field as follows: we assume plasmonic fields with a Gaussian envelope $\mathsf{a}_{\mathrm{SPP}} = \exp[i\varphi]\exp[-\varphi^2/2\omega^2_{\mathrm{SPP}}T^2]$, with $\varphi = k_{\mathrm{SPP}}x - \omega_{\mathrm{SPP}}t$. There are two counterpropagating SPP wave packets, each containing a bright ω_b and a dark ω_d frequency. These terms are multiplied by a "buildup" and "decay" function $f(t) = \exp(-t/2\tau_m) \times \{1 - \mathrm{erf}[(\sigma_m^2 - 2\tau_m t)/(2\sqrt{2}\sigma_m\tau_m)]\}$, which is the convolution of a Gaussian excitation profile with exponential decay. Source duration and plasmon mode decay rate are denoted by σ_m and τ_m, respectively, for $m = b, d$. When $f(t)$ multiplies the plasmonic term, the respective τ_m

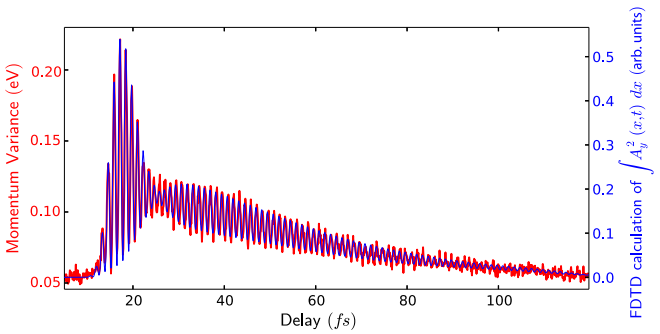

FIG. 2 (color online). Comparison between variance of photoscopic spectrogram in the "filtered isotropic" case (red) and $\int |\mathsf{a}_y|^2 dx$ computed in the FDTD (blue). The offset of the filtered isotropic case is due to the XUV pulse energy width.

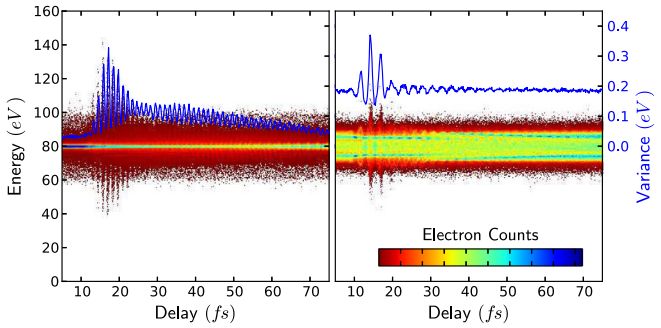

FIG. 3 (color online). Photoscopic spectrograms at perpendicular (left) and grazing (right) electron emission. The measurements retrieve plasmonic and NIR fields, respectively. Solid lines are the momentum variances.

parametrizes the lifetime, while the Gaussian half width at half maximum in intensity $\xi_m = \sigma_m\sqrt{\ln 2}$ parametrizes the buildup time.

The remaining fit parameters are the amplitudes of the respective plasmon modes. The explicit form of the parametrization is given in the Supplemental Material [14]. The relevant free parameters in this model are the excitation buildup times ξ_b, ξ_d, the plasmon decay times τ_b, τ_d and the plasmon frequencies ω_b, ω_d for the bright and dark modes, respectively.

Fitting to the simulated variance, we find plasmon frequencies are $\hbar\omega_b = 1.65$ eV and $\hbar\omega_d = 1.62$ eV, consistent with the plasmonic band gap of 14 nm given in Ref. [16]. Results for the buildup and lifetimes are reported in Table I. Because of spatial integration, the plasmon pulse extension T has little influence on the variance. The values in the table were obtained with $T = 15$ fs (FWHM). A conservative lower bound of T is given by the diameter of the NIR spot size, an upper bound by that size plus plasmon propagation during excitation. Variation in the range of $T = 10$ and 20 fs has only a small effect on buildup and decay times. Because of the superposition of bright mode decay with dark mode buildup, variation is largest for these parameters with about 0.7 fs. For any given value of T in this interval, the buildup and decay extracted from the FDTD surface field and from the spectrogram variance are in good agreement. A comparison of the two spectrograms in Fig. 3 of the NIR vs the plasmonic field allows the evaluation of the field enhancement, which is, in the present case, ~1. From the spectrogram at grazing direction, we get a NIR pulse duration of $\Delta t_{\mathrm{FWHM}} = 4.5$ fs, in good agreement with the 4.6 fs from the FDTD code. Such a measurement provides an independent *in situ* diagnosis of the field distortions of the NIR field caused by the interaction with the grating.

TABLE I. Carrier frequency ω_m, buildup time ξ_m, and lifetime τ_m resulting from fits of the theoretical model to the numerically simulated data. The cases isotropic emission with perpendicular detection ("filtered"), unidirectional emission, as well as values extracted directly from the FDTD calculation are shown. (Times in fs. Frequencies in eV).

	Filtered isotropic	Unidirectional	FDTD
ξ_b	2.07	2.06	2.01
τ_b	3.0	3.1	2.96
ξ_d	6.6	6.2	5.3
τ_d	32.5	33.3	34.6
ω_b	1.61	1.62	1.62
ω_d	1.65	1.65	1.65

In conclusion, we have shown how to obtain, with existing experimental instrumentation, direct, time-resolved images of the SPP surface field. Time resolution is determined by controlling the relative pulse delay. This allows the extraction of basic parameters such as SPP buildup and lifetimes. Attosecond resolution, in our example, provides for the distinction of bright and dark mode oscillations. The same setup also provides *in situ* diagnostics of the NIR pulse.

Once spatially separated XUV attosecond and NIR pulses become available, one may also resolve in space and time other surface phenomena: by letting the NIR field excite a surface mode in some region, one can image SPP propagation along complex plasmonic waveguides or plasmonic switches by simply pointing the attosecond XUV pulse on the region of interest.

We are grateful to C. Ropers for useful discussions. We acknowledge support by the DFG, by the excellence cluster "Munich Center for Advanced Photonics (MAP)," by the Austrian Science Foundation Project No. ViCoM (F41), by the Landesexzellenzcluster "Frontiers in Quantum Photon Science" and the Joachim Herz Stiftung.

*mattia.lupetti@physik.uni-muenchen.de
†armin.scrinzi@lmu.de

[1] E. Ozbay, Science **311**, 189 (2006).
[2] C. Ropers, D. J. Park, G. Stibenz, G. Steinmeyer, J. Kim, D. S. Kim, and C. Lienau, Phys. Rev. Lett. **94**, 113901 (2005).
[3] R. Kienberger, E. Goulielmakis, M. Uiberacker, A. Baltuska, V. Yakovlev, F. Bammer, A. Scrinzi, T. Westerwalbesloh, U. Kleineberg, U. Heinzmann, M. Drescher, and F. Krausz, Nature (London) **427**, 817 (2004).
[4] A. L. Cavalieri, N. Müller, T. Uphues, V. S. Yakovlev, A. Baltuska, B. Horvath, B. Schmidt, L. Blümel, R. Holzwarth, S. Hendel, M. Drescher, U. Kleineberg, P. M. Echenique, R. Kienberger, F. Krausz, and U. Heinzmann, Nature (London) **449**, 1029 (2007).
[5] M. Hentschel, R. Kienberger, C. Spielmann, G. A. Reider, N. Milosevic, T. Brabec, P. Corkum, U. Heinzmann, M. Drescher, and F. Krausz, Nature (London) **414**, 509 (2001).
[6] P. B. Corkum, Phys. Rev. Lett. **71**, 1994 (1993).
[7] P. Agostini and L. F. DiMauro, Rep. Prog. Phys. **67**, 813 (2004).
[8] W. L. Barnes, T. W. Preist, S. C. Kitson, and J. R. Sambles, Phys. Rev. B **54**, 6227 (1996).

[9] F. Süßmann and M. F. Kling, Phys. Rev. B **84**, 121406 (2011).
[10] S. Neppl, R. Ernstorfer, E. M. Bothschafter, A. L. Cavalieri, D. Menzel, J. V. Barth, F. Krausz, R. Kienberger, and P. Feulner, Phys. Rev. Lett. **109**, 087401 (2012).
[11] A. Taflove, *Computational Electrodynamics: The Finite-Difference Time-Domain Method* (Artech House, Boston, 1995).
[12] A. F. Oskooi, D. Roundy, M. Ibanescu, P. Bermel, J. Joannopoulos, and S. G. Johnson, Comput. Phys. Commun. **181**, 687 (2010).
[13] A. D. Rakić, A. B. Djurišić, J. M. Elazar, and M. L. Majewski, Appl. Opt. **37**, 5271 (1998).
[14] See Supplemental Material at http://link.aps.org/supplemental/10.1103/PhysRevLett.113.113903 for a detailed description of the fit and error estimates, which includes Ref. [15].
[15] F. J. Garcia-Vidal, J. Sanchez-Dehesa, A. Dechelette, E. Bustarret, T. Lopez-Rios, T. Fournier, and B. Pannetier, J. Lightwave Technol. **17**, 2191 (1999).
[16] C. Ropers, T. Elsaesser, G. Cerullo, M. Zavelani-Rossi, and C. Lienau, New J. Phys. **9**, 397 (2007).